



1 Clustering diurnal cycles of day-to-day temperature change to 2 understand their impacts on air quality forecasting in mountain- 3 basin areas

4 Debing Kong^{1,2}, Shigong Wang^{3,4}, Guicai Ning^{3,5*}, Jing Cong⁶, Ming Luo^{5,7}, Xiang Ni^{1,2}, Mingguo
5 Ma^{1,2}

6 ¹Chongqing Jinpo Mountain Karst Ecosystem National Observation and Research Station, School of Geographical
7 Sciences, Southwest University, Chongqing, 400715, China

8 ²Chongqing Engineering Research Center for Remote Sensing Big Data Application, School of Geographical Sciences,
9 Southwest University, Chongqing, 400715, China

10 ³The Gansu Key Laboratory of Arid Climate Change and Reducing Disaster, College of Atmospheric Sciences, Lanzhou
11 University, Lanzhou 730000, China

12 ⁴Sichuan Key Laboratory for Plateau Atmosphere and Environment, School of Atmospheric Sciences, Chengdu University
13 of Information Technology, Chengdu 610225, China

14 ⁵Institute of Environment, Energy and Sustainability, The Chinese University of Hong Kong, Shatin, N.T., Hong Kong,
15 China

16 ⁶Tianjin Municipal Meteorological Observatory, Tianjin 300074, China

17 ⁷School of Geography and Planning, and Guangdong Key Laboratory for Urbanization and Geo-simulation, Sun Yat-sen
18 University, Guangzhou 510275, China

19 *Correspondence to: Dr. Guicai Ning (ninggc09@lzu.edu.cn)

20 **Abstract.** Air pollution is substantially modulated by meteorological conditions, and especially their diurnal variations may
21 play a key role in air quality evolution. However, the behaviors of temperature diurnal cycles along with the associated
22 atmospheric condition and their effects on air quality in China remain poorly understood. Here, for the first time we examine
23 the diurnal cycles of day-to-day temperature change and reveal their impacts on winter air quality forecasting in mountain-
24 basin areas. Three different diurnal cycles of the preceding day-to-day temperature change are identified and exhibit notably
25 distinct effects on the day-to-day changes in atmospheric dispersion conditions and air quality. The diurnal cycle with
26 increasing temperature obviously enhances the atmospheric stability in the lower troposphere and suppresses the
27 development of the planetary boundary layer, thus deteriorating the air quality on the following day. By contrast, the diurnal
28 cycle with decreasing temperature in the morning is accompanied by a worse dispersion condition with more stable
29 atmosphere stratification and weaker surface wind speed, thereby substantially worsening the air quality. Conversely, the
30 diurnal cycle with decreasing temperature in the afternoon seems to improve air quality on the following day by enhancing
31 the atmospheric dispersion conditions on the following day. The findings reported here are critical to improve the
32 understanding of air pollution in mountain-basin areas and exhibit promising potential for air quality forecasting.

33



34 1. Introduction

35 Air pollution is not only affected by anthropogenic emissions (Streets et al., 2001; Zhang et al., 2009; Kelly and Zhu, 2016),
36 but also controlled by atmospheric dispersion conditions (Wei et al., 2011; Li et al., 2015; Ye et al., 2016; Zhang et al.,
37 2020). Stagnant meteorological conditions significantly contribute to the formation and maintenance of heavy air pollution
38 as they play important roles in regulating the increment of air pollutants concentrations (Deng et al., 2014; Bei et al., 2016;
39 Zhang et al., 2016; Wang et al., 2018). It is noted that atmospheric dispersion capacity is substantially modulated by synoptic
40 patterns and hence the evolutions of large-scale synoptic systems can lead to the improvement or deterioration of air quality
41 (Yarnal, 1993; Miao et al., 2017; Ning et al., 2019; Dong et al., 2020; Ning et al., 2020). In China, high anthropogenic
42 emissions from coal-fired heating (Xiao et al., 2015), frequent temperature inversion (Xu et al., 2019; Feng et al., 2020; Guo
43 et al., 2020), and shallow planetary boundary layer (PBL) structure (Li et al., 2017; Miao et al., 2018; Su et al., 2020) result
44 in frequent occurrence of heavy air pollution events in winter. These factors highlight the significance of further revealing
45 the physical mechanism of atmospheric dispersion evolutions.

46

47 The behaviors of diurnal cycles of atmospheric dispersion conditions and their effects on air quality remain poorly
48 understood despite air pollution significantly modulated by atmospheric dispersion conditions has been well demonstrated.
49 For instance, as a typical synoptic process occurring in winter in China, the cooling process could cause rapid changes in
50 meteorological and environmental conditions. Cooling processes induce significant day-to-day temperature variations and
51 thus result in substantial changes in air quality (Hu et al., 2018; Ning et al., 2018b; Kang et al., 2019). Many previous studies
52 revealed that cooling processes could remove air pollutants by invading lots of cold fresh airflows (Kalkstein and Corrigan,
53 1986; Gimson, 1994; Hu et al., 2018; Ning et al., 2018b) or exacerbate air pollution by transporting air pollutants (Fu et al.,
54 2008; Ding et al., 2013; Luo et al., 2018; Kang et al., 2019). Nevertheless, most of these studies did not consider the
55 influences of diurnal cycles of cooling processes on air quality. Are the influences of cooling processes occurring during
56 daytime and nighttime on air quality similar or different? The key questions include what are the behaviors of the diurnal
57 cycles of atmospheric dispersion conditions and how these behaviors affect air quality, especially how the diurnal cycles of
58 day-to-day temperature change affect air pollution. Exploring the answers to these questions is critical for fully
59 understanding of winter air pollution and is also urgently needed for improving air quality forecasting in China.

60

61 Sichuan Basin (SCB) is one of the heaviest air pollution areas in China (Zhang et al., 2012; Ning et al., 2018a). With a high
62 population density in SCB, its heavy air pollution thus poses serious health hazards to local residents (Liao et al., 2017; Qiu
63 et al., 2018; Zhu et al., 2018; Zhao et al., 2018). It is noted that SCB has a unique topography, with Qinling-Daba and Wu
64 mountains in the north and east and with Qinghai-Tibet Plateau and Yunnan-Guizhou Plateau in the west and south of the
65 basin (**Fig. 1**). The combination of these complex topography results in unique weather and climate, like the southwest
66 vortex and the Huaxi Autumn rain season etc. The southwest vortex, southern branch, and Qinghai-Tibet high pressure are



67 often formed over SCB or Tibetan plateau and the complex synoptic systems significantly affect atmospheric dispersion
68 conditions (Wang et al., 1993; Wei et al., 2014; Feng et al., 2016; Yu et al., 2016; Ning et al., 2019; Ning et al., 2020).
69 Therefore, both the physical mechanism of atmospheric conditions effects on air pollution and the air quality forecasting in
70 SCB are more complicated than these in the eastern plain regions of China (Chen and Xie, 2012; Wang et al., 2014; Ning et
71 al., 2019; Zhang et al., 2019). To better understand the formation mechanism of air pollution and improve air quality
72 forecasting in mountain-basin areas, the effects of diurnal variations of atmospheric dispersion conditions on winter air
73 quality in SCB call for urgent examinations.

74

75 The scientific goals of this study are to first cluster the typical diurnal cycles of day-to-day temperature change in SCB
76 during wintertime and then to examine the mechanisms underlying the effects of the identified typical diurnal cycles on the
77 following day-to-day air quality changes. Our study is expected to better understand the physical mechanism of air quality
78 evolutions and improve air pollution forecasting in mountain-basin areas. The rest of this paper is organized as below. Data
79 and methodology are introduced in section 2. Section 3 describes the results of our study. Discussion related to our findings
80 is given in section 4. Our conclusions are summarized in section 5.

81 **2. Data and methodology**

82 **2.1 Air quality data**

83 Hourly concentrations of surface $PM_{2.5}$ (particulate matter with an aerodynamic diameter equal to or less than $2.5 \mu m$), PM_{10}
84 (particulate matter with an aerodynamic diameter equal to or less than $10 \mu m$), SO_2 (sulfur dioxide), NO_2 (nitrogen dioxide),
85 and CO (carbon monoxide) in the winters (December–February) from December, 2014 to February, 2020 in 18 cities of SCB
86 (**Fig. 1**) are obtained from the Ministry of Ecology and Environment of the People's Republic of China
87 (<http://www.mee.gov.cn/xxgk2018/>). We calculate the city-wide average concentrations of the five air pollutants by
88 arithmetically averaging their concentration at the national air quality monitoring sites located in the urban areas of that city,
89 based on the technical regulation for ambient air quality assessment (on trial) (MEP, 2013; Ning et al., 2020). Among the 18
90 cities in SCB, ten (Leshan, Meishan, Ziyang, Guangyuan, Bazhong, Ya'an, Dazhou, Suining, Guangan, and Neijiang) began
91 monitoring air quality since January 1, 2015. Hence, the starting date of air quality data for these 10 cities is December 1,
92 2015. The starting date of air quality data for the rest 8 cities (Chengdu, Deyang, Mianyang, Zigong, Yibin, Luzhou,
93 Nanchong and Chongqing) is December 1, 2014.

94 **2.2 Meteorological observational data**

95 Hourly winter surface temperature data observed at 105 meteorological stations in SCB (**Fig. 1**) from December 2006 to
96 February 2020 are also collected. Their regional averages are used to determine the diurnal cycles of day-to-day temperature
97 change. Additionally, daily mean surface wind speed in the 18 cities of SCB is also collected. To explore the thermodynamic



98 structure of the lower troposphere, daily potential temperature profiles at 20:00 Beijing time (BJT, UTC+8 h) from four
99 sounding stations in SCB are also obtained. Four sounding stations, including Chengdu, Yibin, Dazhou, and Chongqing, are
100 located in the northwest, southwest, northeast and southeast of the basin, respectively (See the orange dots in **Fig.1**). All
101 these surface meteorological observations are obtained from the China Meteorological Administration (CMA)
102 (<http://data.cma.cn/data/>).

103 **2.3 ERA-5 reanalysis data**

104 To obtain winter lower troposphere stability, 700 hPa temperature and air pressure and air temperature at 2 m above the
105 ground from December 2014 to February 2020 are collected from daily ERA-5 reanalysis data (0.25°×0.25° grids)
106 (<https://cds.climate.copernicus.eu/cdsapp#!/dataset>). We collect the reanalysis data at four times each day (UTC 00:00,
107 06:00, 12:00 and 18:00) to calculate their daily mean values. The PBL height (PBLH) data at UTC 06:00 (14:00 BJT) are
108 also obtained. PBLH is defined as the lowest model level where the bulk Richardson number first reaches the threshold value
109 of 0.25 (Beljaars, 2006).

110 **2.4 Quantitative measurements of meteorological and air quality variables**

111 **2.4.1 Lower troposphere stability**

112 The lower troposphere stability (LTS) is defined as the differences in potential temperature between 700 hPa and the surface
113 (Slingo, 1987). LTS can describe the thermal state of the lower troposphere and thus can be used to evaluate the vertical
114 mixing of air pollutants in the lower troposphere (Guo et al., 2016a; Guo et al., 2016b). A larger LTS indicates a stronger
115 stability in the lower troposphere and a weaker vertical mixing of air pollutants.

116 **2.4.2 Day-to-day changes in meteorological conditions and air quality**

117 The day-to-day temperature change for each hour of a given day is defined by the hourly temperature differences between
118 two neighboring days (Karl et al., 1995):

$$119 \Delta T = T_i - T_{i-1} \quad (1)$$

120 where ΔT refers to day-to-day temperature change, T_i and T_{i-1} are the hourly temperatures at the specific time of the day and
121 the previous day, respectively.

122
123 To investigate the effects of diurnal cycles of day-to-day temperature change on air quality, we also calculate the day-to-day
124 changes in air pollutants concentrations and atmospheric dispersion conditions following the temperature change within one
125 day. The following day-to-day changes in air pollutants concentrations (or atmospheric dispersion conditions) are defined by
126 the differences in air pollutants concentrations (or meteorological conditions) between the next day and the current day:

$$127 \Delta PC = PC_{i+1} - PC_i \quad (2)$$



128 where PC represents PBLH, LTS, vertical potential temperature profiles (PT), surface wind speed (WS), or the
129 concentrations of $PM_{2.5}$, PM_{10} , SO_2 , NO_2 , and CO. ΔPC represents the following day-to-day changes in PBLH, LTS, PT,
130 WS, and five air pollutants concentrations. PC_{i+1} is the daily mean LTS, WS, and air pollutants concentrations, or the PBLH
131 at 14:00 BJT and PT at 20:00 BJT on the next day. PC_i is the daily mean LTS, WS, and air pollutants concentrations, or the
132 PBLH at 14:00 BJT and PT at 20:00 BJT on the current day.

133 2.5 K-means clustering

134 Clustering methods divide the objects into specific groups, with the goal that all data objects assigned to the same cluster
135 have common characteristics while different clusters have distinct characteristics (Darby, 2005). The clustering methods
136 have been widely used in climate and environmental researches (Bardossy et al., 1995; Cavazos, 2000; Luo and Lau, 2017;
137 Bernier et al., 2019). In this study, the regional average values of day-to-day temperature change in SCB and the K-means
138 clustering method (MacQueen, 1967) are selected to classify the diurnal cycles of day-to-day temperature change, because of
139 the simplicity and convergence characteristics of K-means clustering method. The details of K-means clustering method can
140 refer to MacQueen (1967) and (Mokdad and Haddad, 2017). Additionally, the Calinski-Harabasz criterion, also known as the
141 variance ratio criterion, is utilized to determine the optimal number of clusters (Caliński and Harabasz, 1974). The ultimate
142 goal of Calinski-Harabasz criterion is to maximize the variance measure ratio of homogeneity within a cluster and
143 heterogeneity between clusters (Chikumbo and Granville, 2019).

144

145 3. Results

146 3.1 Diurnal cycles of day-to-day temperature change

147 The selection of optimal number of clusters is illustrated in **Fig. 2**, which shows Calinski-Harabasz values associated with
148 the numbers of clusters ranging from two to ten. The Calinski-Harabasz value with three clusters reaches the highest value,
149 indicating that the optimal number of clustering is three. Three dominant diurnal cycles of day-to-day temperature change
150 are therefore identified in SCB. The three typical diurnal cycles of day-to-day temperature change are depicted in **Fig. 3**. The
151 days for *Cluster 1*, *Cluster 2*, and *Cluster 3* are 455 (accounting for 36.9 % of total days), 413 (33.5%), and 365 days
152 (29.6%), respectively, indicating that the differences in the occurrence frequency among the three diurnal cycles are not
153 noticeable. However, the diurnal cycles of day-to-day temperature change among the three clusters exhibit obvious
154 differences.

155

156 In particular, *Cluster 1* (diurnal cycle with increasing temperature), all the temperature changes are positive for 24 hours
157 throughout all day, indicating that temperature increases during the past 24-hour and exhibits a maximum change
158 approaching 1.5 °C between 16:00 BJT and 17:00 BJT. *Cluster 2* (diurnal cycle with decreasing temperature in the



159 afternoon), the temperature changes show negative values after 12:00 BJT and drop to trough between 16:00 BJT and 17:00
160 BJT with the minimum value of $-1.5\text{ }^{\circ}\text{C}$, indicating that the cooling process is obvious in the afternoon. After 17:00 BJT, the
161 absolute values of temperature change begin to decrease. The most prominent feature of *Cluster 2* is that the obvious
162 decrease in temperature appears in the afternoon. *Cluster 3* (diurnal cycle with decreasing temperature in the morning), all
163 temperature changes are negative for 24 hours throughout all day, and the obviously cooling process appears from 00:00 BJT
164 to 09:00 BJT. The temperature changes show the minimum value approaching $-1.5\text{ }^{\circ}\text{C}$ between 07:00 BJT and 09:00 BJT.
165 After 09:00 BJT, the absolute values of temperature change gradually reduce and are nearly close to zero in the afternoon.
166 The most prominent feature of *Cluster 3* is that the obvious decrease in temperature appears in the morning.

167 3.2 Air quality in relation to the identified diurnal cycles

168 Heavy air pollution during winter in SCB is mainly caused by high concentrations of particulate matter ($\text{PM}_{2.5}$ and PM_{10})
169 (Ning et al., 2018a). Therefore, the day-to-day changes in $\text{PM}_{2.5}$ and PM_{10} concentrations following the three identified
170 diurnal cycles within one day are investigated. **Fig. 4** depicts the spatial distributions of the following day-to-day changes in
171 $\text{PM}_{2.5}$ and PM_{10} concentrations associated with the three typical diurnal cycles. Under the diurnal cycle with increasing
172 temperature (*Cluster 1*), nearly all parts of SCB experience increases in $\text{PM}_{2.5}$ and PM_{10} concentrations on the following day
173 (**Fig. 4a** and **d**). The regional average changes in $\text{PM}_{2.5}$ and PM_{10} concentrations are up to $+3.95\text{ }\mu\text{g}/\text{m}^3$ and $+5.89\text{ }\mu\text{g}/\text{m}^3$,
174 respectively.

175

176 On the contrary, negative changes in $\text{PM}_{2.5}$ and PM_{10} concentrations are observed in the entire basin for the diurnal cycle
177 with decreasing temperature in the afternoon (*Cluster 2*) (**Fig. 4b** and **e**), indicating the improvement of air quality on the
178 following day. The regional average changes in $\text{PM}_{2.5}$ and PM_{10} concentrations are up to $-8.93\text{ }\mu\text{g}/\text{m}^3$ and $-11.50\text{ }\mu\text{g}/\text{m}^3$,
179 respectively. Under the diurnal cycle with decreasing temperature in the morning (*Cluster 3*), all parts of SCB experience
180 increases in $\text{PM}_{2.5}$ and PM_{10} concentrations (**Fig. 4c** and **f**), indicating the deterioration of air quality on the following day. It
181 is noted that opposite changes in $\text{PM}_{2.5}$ and PM_{10} concentrations are observed between *Cluster 3* and *Cluster 2* even though
182 both of the two diurnal cycles show decreasing temperature. Compared with the diurnal cycle with increasing temperature
183 (*Cluster 1*), the increases in $\text{PM}_{2.5}$ and PM_{10} concentrations are larger for *Cluster 3*, and the regional average changes in
184 $\text{PM}_{2.5}$ and PM_{10} concentrations are up to $+5.36\text{ }\mu\text{g}/\text{m}^3$ and $+5.91\text{ }\mu\text{g}/\text{m}^3$, respectively.

185

186 The contributions of gaseous pollutants in SCB to winter air pollution are also very important as SCB has a large number of
187 motor vehicles and industries (Ning et al., 2018a). Therefore, the following day-to-day changes in three major gaseous (SO_2 ,
188 NO_2 , and CO) concentrations associated with the three diurnal cycles are also investigated. Similar to particulate matter, the
189 relationships between the following day-to-day changes in gaseous pollutants concentrations and the three diurnal cycles are
190 consistent with the results showed in **Fig. 4**. As shown in **Fig. 5**, nearly all parts of SCB experience increases in SO_2 , NO_2 ,
191 and CO concentrations on the following day for *Cluster 1* (diurnal cycle with increasing temperature) and *Cluster 3* (diurnal



192 cycle with decreasing temperature in the morning). On the contrary, negative changes in SO₂, NO₂, and CO concentrations
193 are observed in the entire basin for *Cluster 2* (diurnal cycle with decreasing temperature in the afternoon).

194

195 **Figs. 4** and **5** collectively indicate that the air quality in SCB corresponding to *Cluster 1* and *Cluster 3* will deteriorate on the
196 following day, while the air quality corresponding to *Cluster 2* will improve. These results suggest that the modulations of
197 diurnal cycles of day-to-day temperature change on the following day-to-day changes in winter air quality are obvious and
198 important. Thus, the diurnal cycles of day-to-day temperature change exhibit promising potential for winter air quality
199 forecasting on the following day in SCB.

200 3.3 Mechanism of the identified diurnal cycles effects on air quality

201 To reveal the potential influence mechanism of the diurnal cycles of day-to-day temperature change on the following day-to-
202 day changes in air quality, the atmospheric dispersion conditions corresponding to the three identified diurnal cycles are
203 investigated. Firstly, the following day-to-day changes in PT vertical profiles at four sounding stations in SCB (**Fig. 6**) are
204 examined to explore the thermodynamic structure in the lower troposphere. Then, the following day-to-day changes of the
205 three meteorological parameters related to atmospheric dispersion conditions, including LTS (**Fig. 7a–c**), PBLH (**Fig. 7d–f**),
206 and WS (**Fig. 7g–i**) are also investigated to evaluate the evolutions of atmospheric dispersion capacity.

207

208 Under the diurnal cycle with increasing temperature (*Cluster 1*), three sounding stations (Yibin, Dazhou, and Chongqing)
209 experience increases in PT between 950 hPa to 800 hPa on the following day (**Fig. 6d, g, and j**). In Chengdu, decreased PT
210 is observed below 900 hPa, while increased PT appears between 900 hPa to 750 hPa (**Fig. 6a**). All the PT profiles over the
211 four sounding stations show higher temperature change in the level between middle level (800–850 hPa) than the lower level
212 (900–950 hPa), which could enhance the atmospheric stability in the lower troposphere. As shown in **Fig. 7a**, increased LTS
213 are observed in most of the cities in SCB, indicating the atmospheric stratification in the lower troposphere becomes more
214 stable. The stable atmospheric stratification inhibits the vertical mixing of the atmosphere and suppresses the development of
215 PBL (Karppinen et al., 2001; Bei et al., 2016). As shown in **Fig. 7d**, obviously decreased PBLH are observed in all 18 cities
216 of SCB.

217

218 Additionally, we also analyzed the following day-to-day changes in surface wind speed as the wind speed can represent the
219 horizontal dispersion capacity of air pollutants (Lu et al., 2012; Deng et al., 2014). No noticeable decreases in wind speed
220 appear in SCB (**Fig. 7g**). These results suggest that the diurnal cycle with increasing temperature (*Cluster 1*) enhances
221 atmospheric stability in the lower troposphere, which can weaken the vertical exchange of airflow and then suppress the
222 development of PBL, resulting in a small dispersion space of air pollutants and poor air quality in SCB on the following day.
223 Compared with *Cluster 1*, opposite vertical structure of PT changes (**Fig. 6b, e, h, and k**) is observed for the diurnal cycle
224 with decreasing temperature in the afternoon (*Cluster 2*), which could weaken the atmospheric stability in the lower



225 troposphere. As shown in **Fig. 7b**, negative changes in LTS appear in all parts of SCB, enhancing the vertical exchange of
226 airflow and facilitating the development of PBL. As a result, increased PBLH is observed in all parts of SCB (**Fig. 7e**), and
227 the regional average increment is up to 93.0 m. At the same time, the weakened atmospheric stability in the lower
228 troposphere is also conducive to the development of surface wind speed. As shown in **Fig. 7h**, the surface wind speed in the
229 entire SCB is strengthened obviously, indicating the horizontal dispersion capacity of air pollutants is also improved. These
230 results suggest that the diurnal cycle with decreasing temperature in the afternoon weakens atmospheric stability in the lower
231 troposphere and creates good vertical mixing of airflow, which can promote the development of PBL and surface wind
232 speed, facilitating the improvement of air quality on the following day.

233

234 For the Cluster 3, the PT changes are not noticeable below 850 hPa over the four sounding stations. As shown in **Fig. 6c, f, i**,
235 and **l**, decreased PT is observed between 850 hPa and 700 hPa, while obviously increased PT appears above 700 hPa. This
236 vertical structure of PT changes suggests that the atmospheric stability is enhanced above PBL over SCB, which is
237 demonstrated playing key role in the formation of winter heavy air pollution events in the basin (Ning et al., 2018b; Ning et
238 al., 2019). As shown in **Fig. 7c**, increased LTS appears in the entire SCB, and the increments of LTS are obviously larger
239 than those for *Cluster 1* (**Fig. 7a**), inhibiting the vertical mixing of atmosphere and suppressing the development of PBL. As
240 a result, decreased PBLH is observed in all parts of SCB. Compared with *Cluster 1*, the enhanced atmospheric stability
241 above PBL also suppresses the development of surface wind speed. As shown in **Fig. 7i**, all parts of SCB experience
242 decreases in surface wind speed, weakening the horizontal dispersion capacity of air pollutants. These results suggest that
243 both the vertical and horizontal dispersion capacity of air pollutants corresponding to *Cluster 3* are worse than those
244 corresponding to *Cluster 1*. The differences in the atmospheric dispersion conditions between *Cluster 3* and *Cluster 1* can
245 explain well that the air quality deterioration is more serious for *Cluster 3* than *Cluster 1* (**Fig. 4** and **Fig. 5**).

246 4. Discussion

247 It's worth noting that the following day-to-day air quality changes between *Cluster 2* and *Cluster 3* in mountain-basin areas
248 are opposite, even though both of the two diurnal cycles are associated with cooling processes. In the cases of the cooling
249 process mainly occurring in the afternoon (*Cluster 2*), the atmospheric dispersion conditions are obviously improved,
250 resulting in air quality improvement on the following day. On the contrary, the atmospheric dispersion conditions are
251 obviously inhibited when the cooling process mainly appears in the morning (*Cluster 3*), resulting in air quality deterioration
252 on the following day. These findings could improve our understanding of the effects of cooling processes on air quality
253 (Kalkstein and Corrigan, 1986; Gimson, 1994; Hu et al., 2018; Ning et al., 2018b; Kang et al., 2019) and suggest that
254 comprehensive investigations for the effects of diurnal cycles of atmospheric dispersion conditions on air quality are
255 urgently needed in the future to fully understand the physical mechanism of air quality evolutions.

256



257 Additionally, both *Cluster 1* and *Cluster 3* are associated with weakened atmospheric dispersion conditions and lead to air
258 quality deterioration on the following day. However, obvious differences in PT vertical profiles (**Fig. 6**) between *Cluster 1*
259 and *Cluster 3* are observed. Especially for *Cluster 3*, decreased PT is observed between 850 hPa and 700 hPa, while
260 obviously increased PT appears above 700 hPa (**Fig. 6c, f, i, and l**). This special vertical structure of PT is closely related to
261 the foehn that is formed under the synergistic effects of cooling processes and the Tibetan Plateau (Ning et al., 2019),
262 indicating a stable layer exists above PBL and acts as a lid covering the PBL (Ning et al., 2018b; Ning et al., 2019). The
263 vertical structure of PT are demonstrated playing key roles in the formation of winter heavy air pollution events in mountain-
264 basin areas by inhibiting the development of secondary circulation and PBL (Ning et al., 2018b; Ning et al., 2019). These
265 features suggest that the physical processes related to air pollution are more complex in mountain-basin areas than in the
266 areas with flat terrain and urgently need to be further explored in the future.

267

268 Our study highlights that the following day-to-day air quality changes in mountain-basin areas are notably affected by the
269 diurnal cycles of day-to-day temperature changes. We find that the identified diurnal cycles of day-to-day temperature
270 variation in our study can explain well the evolutions of atmospheric dispersion conditions and air quality on the following
271 day and thus could be useful for air quality forecasting in mountain-basin areas. Currently, numerical models (including
272 WRF-Chem model and CMAQ model) (Grell et al., 2005; Byun and Ching, 1999) and statistical models (including statistical
273 analysis, machine learning, and the hybrid linear–nonlinear method, etc.) (Huang, 1992; Chelani and Devotta, 2006; Borse,
274 2020) are the two typical methods that have been widely used to forecast air quality by combining weather conditions and
275 emission sources (Gidhagen et al., 2005). In the future, our findings should therefore be combined with numerical models or
276 statistical models to improve air quality forecasting in mountain-basin areas.

277 **5. Conclusions**

278 Taking SCB as an example, this study is the first examination of the behaviors of diurnal cycles of day-to-day temperature
279 change using hourly temperature observations and their effects on the following day-to-day air quality changes in mountain-
280 basin areas. Three diurnal cycles of day-to-day temperature change are identified, which notably affect the following day-to-
281 day air quality changes. Among them, two diurnal cycles (i.e., *Clusters 1 & 3*) inhibit atmospheric dispersion conditions by
282 enhancing atmospheric stability, suppressing PBL, and weakening surface wind speed, thus leading to air quality
283 deterioration on the following day.

284

285 Compared with the diurnal cycle with increasing temperature (i.e., *Cluster 1*), the atmospheric dispersion conditions are
286 worse for the diurnal cycle with decreasing temperature in the morning (i.e., *Cluster 3*) and cause more serious deterioration
287 of air quality. On the contrary, atmospheric dispersion condition with weakened atmospheric stability, deepened PBL, and
288 enhanced surface wind speed is obviously improved for this type of diurnal cycle with decreasing temperature in the



289 afternoon (i.e., *Cluster 2*), which improves the air quality on the following day. These results suggest that the identified
290 diurnal cycles can explain well the evolutions of atmospheric dispersion conditions and air quality on the following day. Our
291 findings exhibit promising potential for air quality forecasting in mountain-basin areas.

292 **Data availability**

293 The hourly air quality data, the meteorological observation data, and the ERA-5 reanalysis data were obtained from the
294 websites described in Sections. 2.1–2.4 and from the scientists listed in the acknowledgement. They are available from these
295 upon request.

296 **Author contributions**

297 DK performed data analysis, prepared the figures, and wrote original draft with contributions from all co-authors. GN
298 designed the research and wrote the manuscript. SW, ML, XN, and MM provided interpretation and editing of the
299 manuscript. JC performed data analysis and provided useful comments.

300 **Competing interests**

301 The authors declare that they have no conflict of interest.

302 **Acknowledgements**

303 This work was supported by the National Natural Science Foundation of China (91644226, 41871029, 41830648, and
304 41771453), the Major Scientific and Technological Projects in Sichuan Province (2018SZDZX0023), the Applied Basic
305 Research Project of Sichuan Science and Technology Department (2020YJ0425), the Technology Innovation Research and
306 Development Project of Chengdu Science and Technology Department (2018-YF05-00219-SN), the National Major Projects
307 on High-Resolution Earth Observation System (21-Y20B01-9001-19/22), and the appointment of M. Luo at Sun Yat-sen
308 University is partially supported by the Pearl River Talent Recruitment Program of Guangdong Province, China
309 (2017GC010634). We would like to thank the following departments for the provided data, the Ministry of Ecology and
310 Environment of the People's Republic of China, the China Meteorological Administration, and the European Centre for
311 Medium-Range Weather Forecasts.



312 References

- 313 Bardossy, A., Duckstein, L., and Bogardi, I.: Fuzzy rule-based classification of atmospheric circulation patterns, *Int. J.*
314 *Climatol.*, 15, 1087-1097, doi: 10.1002/joc.3370151003, 1995.
- 315 Bei, N., Xiao, B., Meng, N., and Feng, T.: Critical role of meteorological conditions in a persistent haze episode in the
316 Guanzhong basin, China, *Sci. Total Environ.*, 550, 273-284, doi: 10.1016/j.scitotenv.2015.12.159, 2016.
- 317 Beljaars, A.: Chapter 3: Turbulent transport and interactions with the surface, Part IV: physical processes, IFS
318 documentation, operational implementation 12 September 2006 Cy31r1 31, ECMWF, Shinfield Park, Reading, RG2 9AX,
319 England, 2006.
- 320 Bernier, C., Wang, Y., Estes, M., Lei, R., Jia, B., Wang, S.-C., and Sun, J.: Clustering surface ozone diurnal cycles to
321 understand the impact of circulation patterns in Houston, TX, *J. Geophys. Res. Atmos.*, 124, 13457-13474, doi:
322 10.1029/2019JD031725, 2019.
- 323 Borse, S. K.: A Review: predicting air quality using different technique, *Acta technica corviniensis-bulletin of engineering*,
324 13, 153-157, 2020.
- 325 Byun, D., and Ching, J.: Science algorithms of the EPA models-3 community multiscale air quality model (CMAQ)
326 modeling system, Rep. EPA/600/R-99, U.S. Environmental Protection Agency, Research Triangle Park, NC, 1999.
- 327 Caliński, T., and Harabasz, J.: A dendrite method for cluster analysis, *Communications in Statistics*, 3, 1-27, doi:
328 10.1080/03610927408827101, 1974.
- 329 Cavazos, T.: Using self-organizing maps to investigate extreme climate events: an application to wintertime precipitation in
330 the Balkans, *J. Clim.*, 13, 1718-1732, doi: 10.1175/1520-0442(2000)013<1718:USOMTI>2.0.CO;2, 2000.
- 331 Chelani, A. B., and Devotta, S.: Air quality forecasting using a hybrid autoregressive and nonlinear model, *Atmos. Environ.*,
332 40, 1774-1780, doi: 10.1016/j.atmosenv.2005.11.019, 2006.
- 333 Chen, Y., and Xie, S.: Temporal and spatial visibility trends in the Sichuan Basin, China, 1973 to 2010, *Atmos. Res.*, 112,
334 25-34, doi: 10.1016/j.atmosres.2012.04.009, 2012.
- 335 Chikumbo, O., and Granville, V.: Optimal clustering and cluster identity in understanding high-dimensional data spaces with
336 tightly distributed points, *Mach. Learn. Knowl. Extr.*, 1, 715-744, doi: 10.3390/make1020042, 2019.
- 337 Darby, L. S.: Cluster analysis of surface winds in Houston, Texas, and the impact of wind patterns on ozone, *J. Appl.*
338 *Meteorol. Climatol.*, 44, 1788-1806, doi: 10.1175/JAM2320.1, 2005.
- 339 Deng, T., Wu, D., Deng, X., Tan, H., Li, F., and Liao, B.: A vertical sounding of severe haze process in Guangzhou area,
340 *Sci. China Earth Sci.*, 57, 2650-2656, doi: 10.1007/s11430-014-4928-y, 2014.
- 341 Ding, A., Wang, T., and Fu, C.: Transport characteristics and origins of carbon monoxide and ozone in Hong Kong, South
342 China, *J. Geophys. Res. Atmos.*, 118, 9475-9488, doi: 10.1002/jgrd.50714, 2013.



- 343 Dong, Y., Li, J., Guo, J., Jiang, Z., Chu, Y., Chang, L., Yang, Y., and Liao, H.: The impact of synoptic patterns on
344 summertime ozone pollution in the North China Plain, *Sci. Total Environ.*, 735, 139559, doi:
345 10.1016/j.scitotenv.2020.139559, 2020.
- 346 Feng, X., Liu, C., Fan, G., Liu, X., and Feng, C.: Climatology and structures of southwest vortices in the NCEP climate
347 forecast system reanalysis, *J. Clim.*, 29, 7675-7701, doi: 10.1175/JCLI-D-15-0813.1, 2016.
- 348 Feng, X., Wei, S., and Wang, S.: Temperature inversions in the atmospheric boundary layer and lower troposphere over the
349 Sichuan Basin, China: climatology and impacts on air pollution, *Sci. Total Environ.*, 726, 138579, doi:
350 10.1016/j.scitotenv.2020.138579, 2020.
- 351 Fu, Q., Zhuang, G., Wang, J., Xu, C., Huang, K., Li, J., Hou, B., Lu, T., and Streets, D. G.: Mechanism of formation of the
352 heaviest pollution episode ever recorded in the Yangtze River Delta, China, *Atmos. Environ.*, 42, 2023-2036, doi:
353 10.1016/j.atmosenv.2007.12.002, 2008.
- 354 Gidhagen, L., Johansson, C., Langner, J., and Foltescu, V. L.: Urban scale modeling of particle number concentration in
355 Stockholm, *Atmos. Environ.*, 39, 1711-1725, doi: 10.1016/j.atmosenv.2004.11.042, 2005.
- 356 Gimson, N. R.: Dispersion and removal of pollutants during the passage of an atmospheric frontal system, *Q. J. R. Meteorol.*
357 *Soc.*, 120, 139-160, doi: 10.1002/qj.49712051509, 1994.
- 358 Grell, G. A., Peckham, S. E., Schmitz, R., McKeen, S. A., Frost, G., Skamarock, W. C., and Eder, B.: Fully coupled “online”
359 chemistry within the WRF model, *Atmos. Environ.*, 39, 6957-6975, doi: 10.1016/j.atmosenv.2005.04.027, 2005.
- 360 Guo, J., Deng, M., Lee, S. S., Wang, F., Li, Z., Zhai, P., Liu, H., Lv, W., Yao, W., and Li, X.: Delaying precipitation and
361 lightning by air pollution over the Pearl River Delta. Part I: observational analyses, *J. Geophys. Res. Atmos.*, 121, 6472-
362 6488, doi: 10.1002/2015JD023257, 2016a.
- 363 Guo, J., Miao, Y., Zhang, Y., Liu, H., Li, Z., Zhang, W., He, J., Lou, M., Yan, Y., Bian, L., and Zhai, P.: The climatology of
364 planetary boundary layer height in China derived from radiosonde and reanalysis data, *Atmos. Chem. Phys.*, 16, 13309-
365 13319, doi: 10.5194/acp-16-13309-2016, 2016b.
- 366 Guo, J., Chen, X., Su, T., Liu, L., Zheng, Y., Chen, D., Li, J., Xu, H., Lv, Y., and He, B.: The climatology of lower
367 tropospheric temperature inversions in China from radiosonde measurements: roles of black carbon, local meteorology,
368 and large-scale subsidence, *J. Clim.*, 33, 9327-9350, doi: 10.1175/JCLI-D-19-0278.1, 2020.
- 369 Hu, Y., Wang, S., Ning, G., Zhang, Y., Wang, J., and Shang, Z.: A quantitative assessment of the air pollution purification
370 effect of a super strong cold-air outbreak in January 2016 in China, *Air Qual. Atmos. Hlth.*, 11, 907-923, doi:
371 10.1007/s11869-018-0592-2, 2018.
- 372 Huang, G.: A stepwise cluster analysis method for predicting air quality in an urban environment, *Atmos. Environ. Part B.*
373 *Urb. Atmos.*, 26, 349-357, doi: 10.1016/0957-1272(92)90010-P, 1992.
- 374 Kalkstein, L. S., and Corrigan, P.: A Synoptic climatological approach for geographical analysis: assessment of sulfur
375 dioxide concentrations, *Ann. Assoc. Am. Geogr.*, 76, 381-395, doi: 10.1111/j.1467-8306.1986.tb00126.x, 1986.



- 376 Kang, H., Zhu, B., Gao, J., He, Y., Wang, H., Su, J., Pan, C., Zhu, T., and Yu, B.: Potential impacts of cold frontal passage
377 on air quality over the Yangtze River Delta, China, *Atmos. Chem. Phys.*, 19, 3673-3685, doi: 10.5194/acp-19-3673-2019,
378 2019.
- 379 Karl, T. R., Knight, R. W., and Plummer, N.: Trends in high-frequency climate variability in the twentieth century, *Nature*,
380 377, 217-220, doi: 10.1038/377217a0, 1995.
- 381 Karppinen, A., Joffre, S. M., Kukkonen, J., and Bremer, P.: Evaluation of inversion strengths and mixing heights during
382 extremely stable atmospheric stratification, *Int. J. Environ. Pollut.*, 16, 603-613, doi: 10.1504/IJEP.2001.000653, 2001.
- 383 Kelly, F. J., and Zhu, T.: Transport solutions for cleaner air, *Science*, 352, 934-936, doi: 10.1126/science.aaf3420, 2016.
- 384 Li, Y., Chen, Q., Zhao, H., Wang, L., and Tao, R.: Variations in PM₁₀, PM_{2.5} and PM_{1.0} in an urban area of the Sichuan Basin
385 and their relation to meteorological factors, *Atmosphere*, 6, 150-163, 2015.
- 386 Li, Z., Guo, J., Ding, A., Liao, H., Liu, J., Sun, Y., Wang, T., Xue, H., Zhang, H., and Zhu, B.: Aerosol and boundary-layer
387 interactions and impact on air quality, *Natl. Sci. Rev.*, 4, 810-833, doi: 10.1093/nsr/nwx117, 2017.
- 388 Liao, T., Wang, S., Ai, J., Gui, K., Duan, B., Zhao, Q., Zhang, X., Jiang, W., and Sun, Y.: Heavy pollution episodes,
389 transport pathways and potential sources of PM_{2.5} during the winter of 2013 in Chengdu (China), *Sci. Total Environ.*, 584-
390 585, 1056-1065, doi: 10.1016/j.scitotenv.2017.01.160, 2017.
- 391 Lu, C., Deng, Q.-h., Liu, W.-w., Huang, B.-l., and Shi, L.-z.: Characteristics of ventilation coefficient and its impact on
392 urban air pollution, *J. Cent. South Univ.*, 19, 615-622, doi: 10.1007/s11771-012-1047-9, 2012.
- 393 Luo, M., and Lau, N.-C.: Heat waves in southern China: synoptic behavior, long-term change, and urbanization effects, *J.*
394 *Clim.*, 30, 703-720, doi: 10.1175/JCLI-D-16-0269.1, 2017.
- 395 Luo, M., Hou, X., Gu, Y., Lau, N.-C., and Yim, S. H.-L.: Trans-boundary air pollution in a city under various atmospheric
396 conditions, *Sci. Total Environ.*, 618, 132-141, doi: 10.1016/j.scitotenv.2017.11.001, 2018.
- 397 MacQueen, J.: Some methods for classification and analysis of multivariate observations, *Proceedings of the fifth Berkeley*
398 *symposium on mathematical statistics and probability*, 1967, 281-297.
- 399 MEP: Technical regulation on ambient air quality assessment (on trial) (HJ663-2013), China Environmental Science Press,
400 Beijing, China, 2013.
- 401 Miao, Y., Guo, J., Liu, S., Liu, H., Li, Z., Zhang, W., and Zhai, P.: Classification of summertime synoptic patterns in Beijing
402 and their associations with boundary layer structure affecting aerosol pollution, *Atmos. Chem. Phys.*, 17, 3097-3110, doi:
403 10.5194/acp-17-3097-2017, 2017.
- 404 Miao, Y., Liu, S., Guo, J., Huang, S., Yan, Y., and Lou, M.: Unraveling the relationships between boundary layer height and
405 PM_{2.5} pollution in China based on four-year radiosonde measurements, *Environ. Pollut.*, 243, 1186-1195, doi:
406 10.1016/j.envpol.2018.09.070, 2018.
- 407 Mokdad, F., and Haddad, B.: Improved infrared precipitation estimation approaches based on k-means clustering:
408 application to north Algeria using MSG-SEVIRI satellite data, *Adv. Space Res.*, 59, 2880-2900, doi:
409 10.1016/j.asr.2017.03.027, 2017.



- 410 Ning, G., Wang, S., Ma, M., Ni, C., Shang, Z., Wang, J., and Li, J.: Characteristics of air pollution in different zones of
411 Sichuan Basin, China, *Sci. Total Environ.*, 612, 975-984, doi: 10.1016/j.scitotenv.2017.08.205, 2018a.
- 412 Ning, G., Wang, S., Yim, S. H. L., Li, J., Hu, Y., Shang, Z., Wang, J., and Wang, J.: Impact of low-pressure systems on
413 winter heavy air pollution in the northwest Sichuan Basin, China, *Atmos. Chem. Phys.*, 18, 13601-13615, doi:
414 10.5194/acp-18-13601-2018, 2018b.
- 415 Ning, G., Yim, S. H. L., Wang, S., Duan, B., Nie, C., Yang, X., Wang, J., and Shang, K.: Synergistic effects of synoptic
416 weather patterns and topography on air quality: a case of the Sichuan Basin of China, *Clim. Dyn.*, 53, 6729-6744,
417 doi:10.1007/s00382-019-04954-3, 2019.
- 418 Ning, G., Yim, S. H. L., Yang, Y., Gu, Y., and Dong, G.: Modulations of synoptic and climatic changes on ozone pollution
419 and its health risks in mountain-basin areas, *Atmos. Environ.*, 240, 117808, doi: 10.1016/j.atmosenv.2020.117808, 2020.
- 420 Qiu, H., Yu, H., Wang, L., Zhu, X., Chen, M., Zhou, L., Deng, R., Zhang, Y., Pu, X., and Pan, J.: The burden of overall and
421 cause-specific respiratory morbidity due to ambient air pollution in Sichuan Basin, China: a multi-city time-series
422 analysis, *Environ. Res.*, 167, 428-436, doi: 10.1016/j.envres.2018.08.011, 2018.
- 423 Slingo, J. M.: The development and verification of a cloud prediction scheme for the ECMWF model, *Q. J. Roy. Meteor.*
424 *Soc.*, 113, 899-927, doi: 10.1002/qj.49711347710, 1987.
- 425 Streets, D. G., Gupta, S., Waldhoff, S. T., Wang, M. Q., Bond, T. C., and Yiyun, B.: Black carbon emissions in China,
426 *Atmos. Environ.*, 35, 4281-4296, doi: 10.1016/S1352-2310(01)00179-0, 2001.
- 427 Su, T., Li, Z., Zheng, Y., Luan, Q., and Guo, J.: Abnormally shallow boundary layer associated with severe air pollution
428 during the COVID-19 lockdown in China, *Geophys. Res. Lett.*, 47, e2020GL090041, doi: 10.1029/2020GL090041, 2020.
- 429 Wang, W., Kuo, Y.-H., and Warner, T. T.: A diabatically driven mesoscale vortex in the lee of the Tibetan Plateau, *Mon.*
430 *Weather Rev.*, 121, 2542-2561, doi: 10.1175/1520-0493(1993)121<2542:ADDMVI>2.0.CO;2, 1993.
- 431 Wang, X., Dickinson, R. E., Su, L., Zhou, C., and Wang, K.: PM_{2.5} pollution in China and how it has been exacerbated by
432 terrain and meteorological conditions, *Bull. Am. Meteorol. Soc.*, 99, 105-119, doi: 10.1175/BAMS-D-16-0301.1, 2018.
- 433 Wang, Y., Yao, L., Wang, L., Liu, Z., Ji, D., Tang, G., Zhang, J., Sun, Y., Hu, B., and Xin, J.: Mechanism for the formation
434 of the January 2013 heavy haze pollution episode over central and eastern China, *Sci. China Earth Sci.*, 57, 14-25, doi:
435 10.1007/s11430-013-4773-4, 2014.
- 436 Wei, P., Cheng, S., Li, J., and Su, F.: Impact of boundary-layer anticyclonic weather system on regional air quality, *Atmos.*
437 *Environ.*, 45, 2453-2463, doi: 10.1016/j.atmosenv.2011.01.045, 2011.
- 438 Wei, W., Zhang, R., Wen, M., Rong, X., and Li, T.: Impact of Indian summer monsoon on the South Asian High and its
439 influence on summer rainfall over China, *Clim. Dyn.*, 43, 1257-1269, doi: 10.1007/s00382-013-1938-y, 2014.
- 440 Xiao, Q., Ma, Z., Li, S., and Liu, Y.: The impact of winter heating on air pollution in China, *PLoS One*, 10, e0117311, doi:
441 10.1371/journal.pone.0117311, 2015.

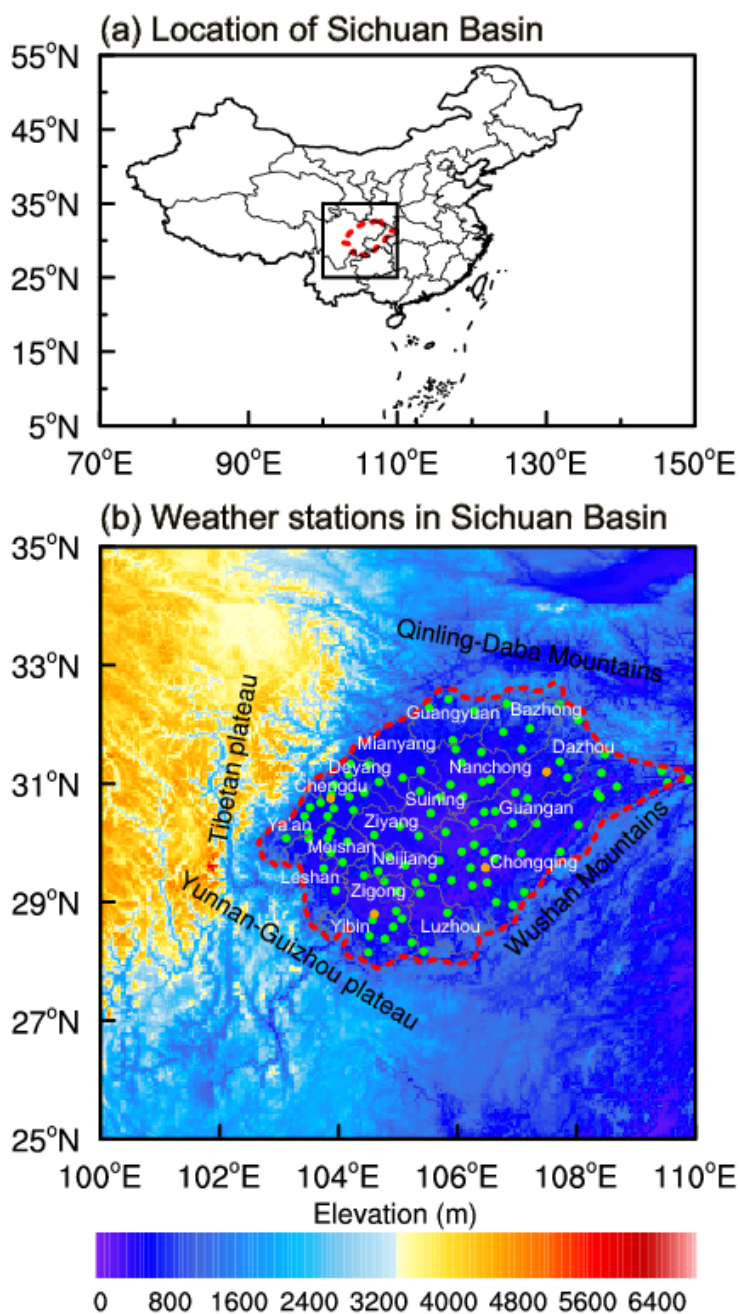


- 442 Xu, T., Song, Y., Liu, M., Cai, X., Zhang, H., Guo, J., and Zhu, T.: Temperature inversions in severe polluted days derived
443 from radiosonde data in North China from 2011 to 2016, *Sci. Total Environ.*, 647, 1011-1020, doi:
444 10.1016/j.scitotenv.2018.08.088, 2019.
- 445 Yarnal, B.: *Synoptic climatology in environmental analysis: a primer*, Belhaven Press, London, 1993.
- 446 Ye, X., Song, Y., Cai, X., and Zhang, H.: Study on the synoptic flow patterns and boundary layer process of the severe haze
447 events over the North China Plain in January 2013, *Atmos. Environ.*, 124, 129-145, doi: 10.1016/j.atmosenv.2015.06.011,
448 2016.
- 449 Yu, S., Gao, W., Xiao, D., and Peng, J.: Observational facts regarding the joint activities of the southwest vortex and plateau
450 vortex after its departure from the Tibetan Plateau, *Adv. Atmos. Sci.*, 33, 34-46, doi :10.1007/s00376-015-5039-1, 2016.
- 451 Zhang, L., Guo, X., Zhao, T., Gong, S., Xu, X., Li, Y., Luo, L., Gui, K., Wang, H., Zheng, Y., and Yin, X.: A modelling
452 study of the terrain effects on haze pollution in the Sichuan Basin, *Atmos. Environ.*, 196, 77-85, doi:
453 10.1016/j.atmosenv.2018.10.007, 2019.
- 454 Zhang, Q., Streets, D. G., Carmichael, G. R., He, K. B., Huo, H., Kannari, A., Klimont, Z., Park, I. S., Reddy, S., Fu, J. S.,
455 Chen, D., Duan, L., Lei, Y., Wang, L. T., and Yao, Z. L.: Asian emissions in 2006 for the NASA INTEX-B mission,
456 *Atmos. Chem. Phys.*, 9, 5131-5153, doi: 10.5194/acp-9-5131-2009, 2009.
- 457 Zhang, X. Y., Wang, Y. Q., Niu, T., Zhang, X. C., Gong, S. L., Zhang, Y. M., and Sun, J. Y.: Atmospheric aerosol
458 compositions in China: spatial/temporal variability, chemical signature, regional haze distribution and comparisons with
459 global aerosols, *Atmos. Chem. Phys.*, 12, 779-799, doi: 10.5194/acp-12-779-2012, 2012.
- 460 Zhang, Y., Guo, J., Yang, Y., Wang, Y., and Yim, S. H. L.: Vertical wind shear modulates particulate matter pollutions: A
461 perspective from radar wind profiler observations in Beijing, China, *Remote Sens.*, 12, 546, 2020.
- 462 Zhang, Z., Zhang, X., Gong, D., Kim, S. J., Mao, R., and Zhao, X.: Possible influence of atmospheric circulations on winter
463 haze pollution in the Beijing–Tianjin–Hebei region, northern China, *Atmos. Chem. Phys.*, 16, 561-571, doi: 10.5194/acp-
464 16-561-2016, 2016.
- 465 Zhao, S., Yu, Y., Yin, D., Qin, D., He, J., and Dong, L.: Spatial patterns and temporal variations of six criteria air pollutants
466 during 2015 to 2017 in the city clusters of Sichuan Basin, China, *Sci. Total Environ.*, 624, 540-557, doi:
467 10.1016/j.scitotenv.2017.12.172, 2018.
- 468 Zhu, S., Xia, L., Wu, J., Chen, S., Chen, F., Zeng, F., Chen, X., Chen, C., Xia, Y., Zhao, X., and Zhang, J.: Ambient air
469 pollutants are associated with newly diagnosed tuberculosis: a time-series study in Chengdu, China, *Sci. Total Environ.*,
470 631-632, 47-55, doi: 10.1016/j.scitotenv.2018.03.017, 2018.

471
472

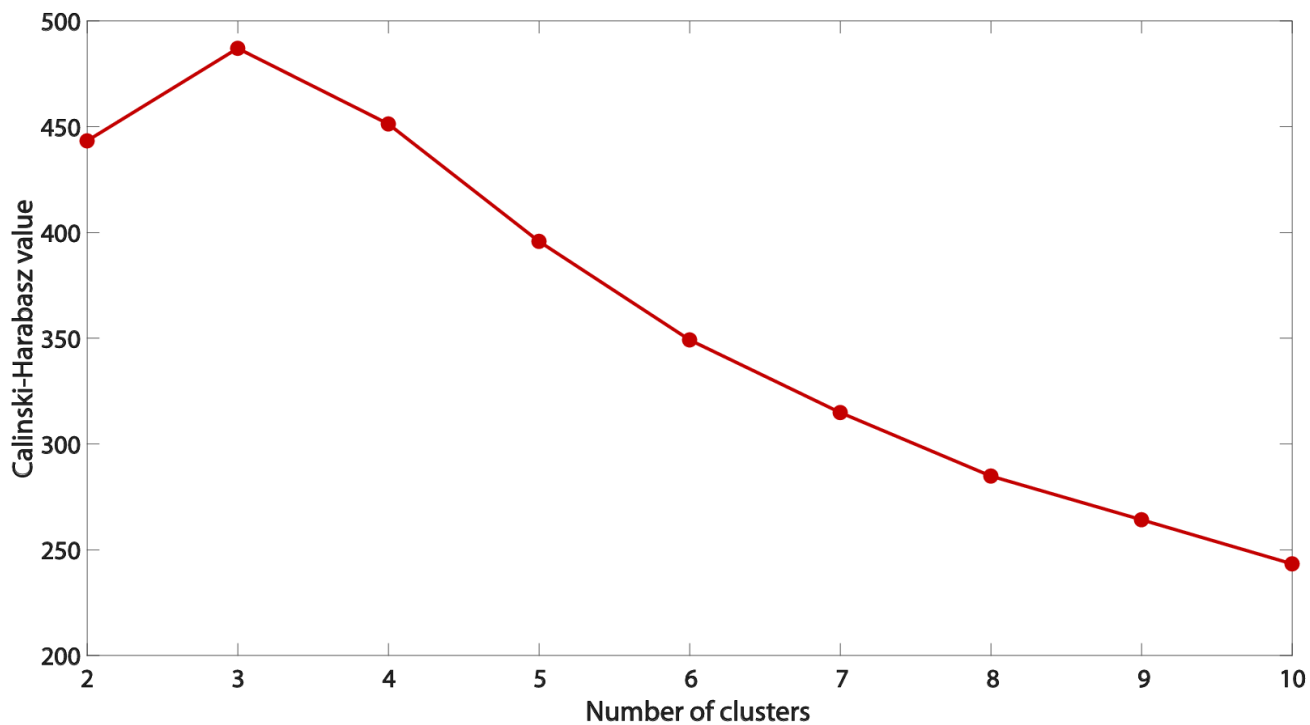


473 **Figures**



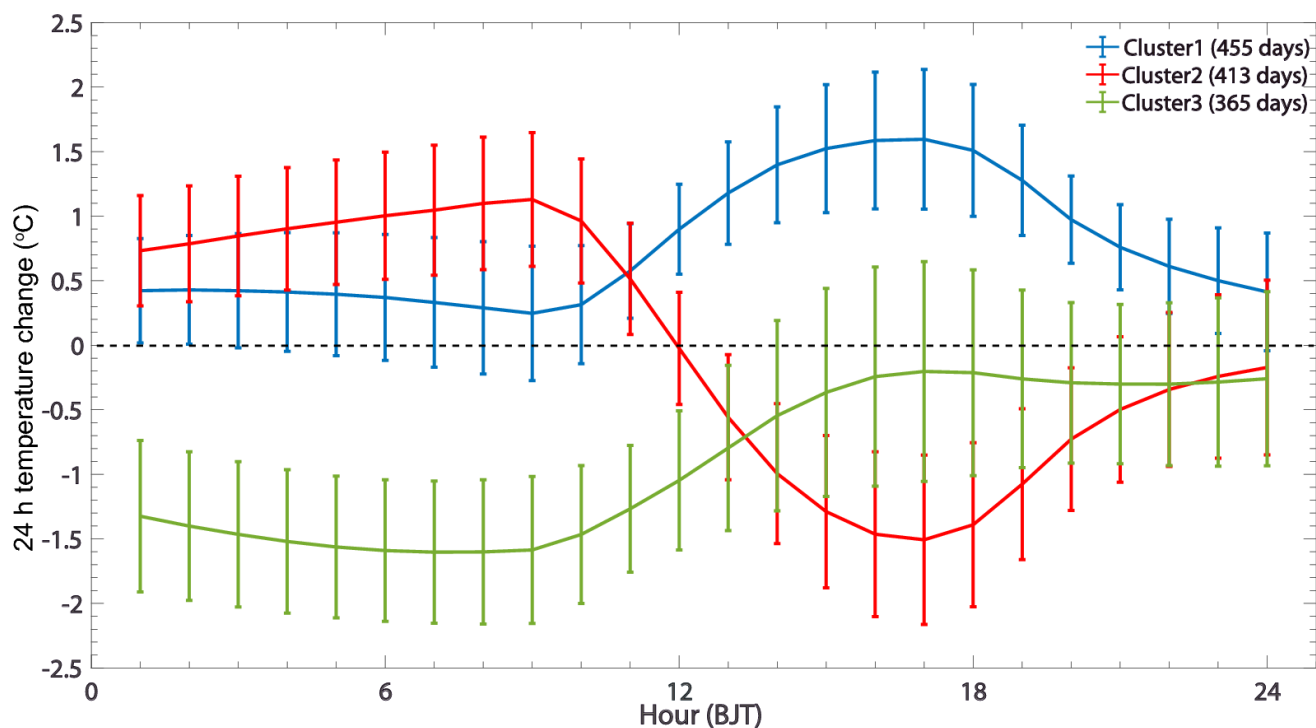
474

475 **Figure 1** Map of Sichuan Basin (SCB) in Southwest China. (a) Location of SCB; (b) Topography of SCB (shading) and the
476 spatial distribution of 105 meteorological stations (dots) in SCB. The dashed red line indicates the border of SCB. The
477 orange dots indicate the meteorological stations with radiosonde measurements.



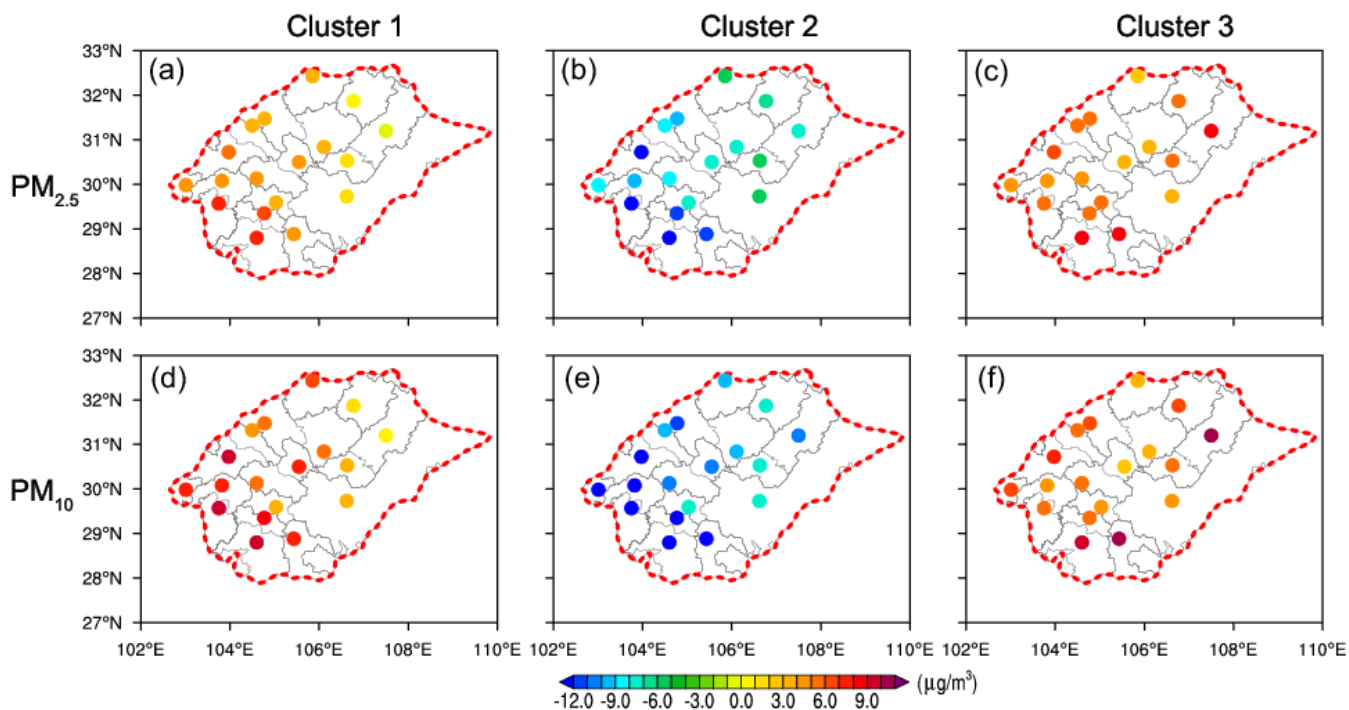
478

479 **Figure 2** Changes of Calinski-Harabasz values with different numbers of identified clusters.



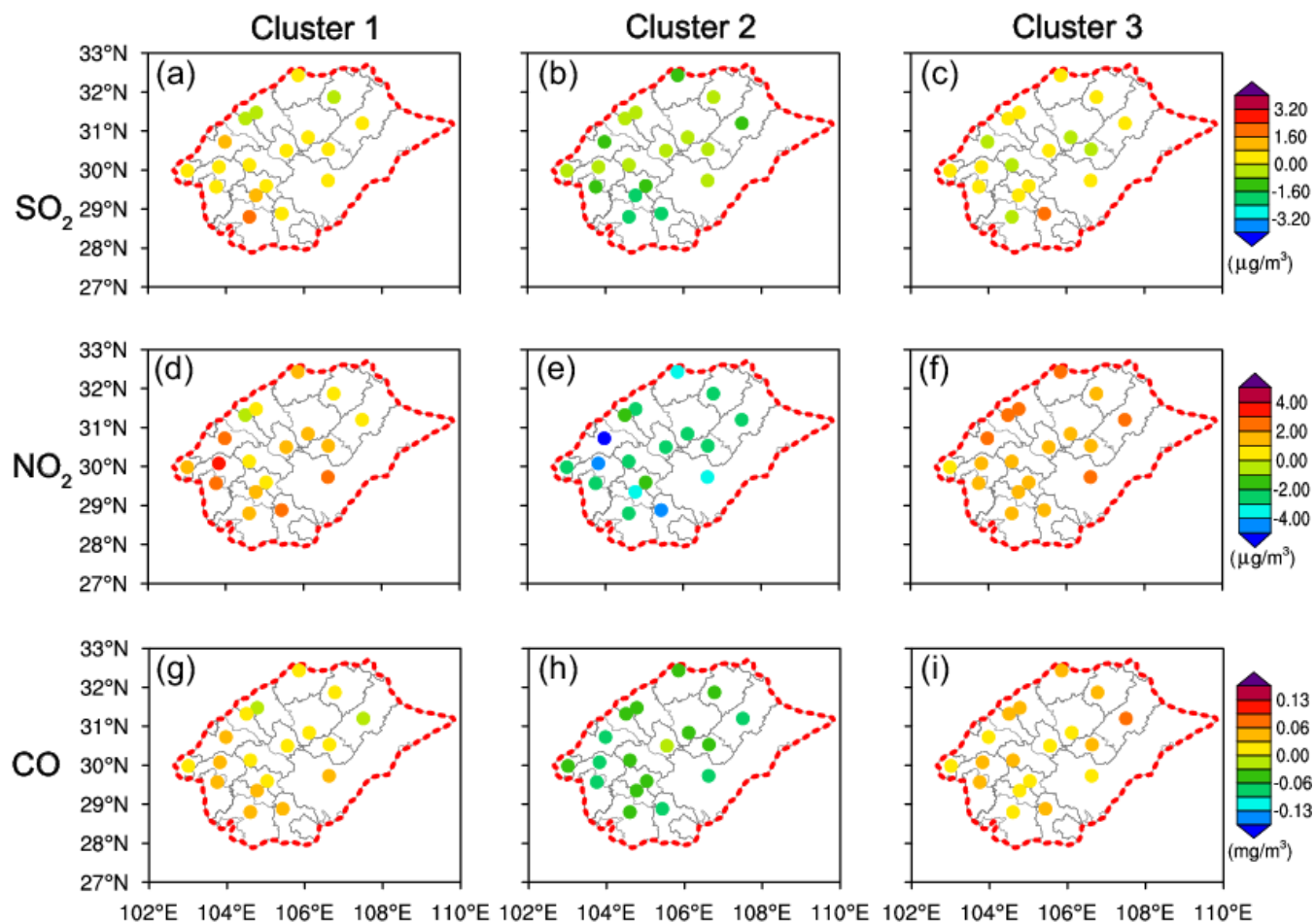
480

481 **Figure 3** Three identified diurnal cycles of day-to-day temperature change based on the K-means clustering method. The
482 error bar denotes the standard deviation of day-to-day temperature change.



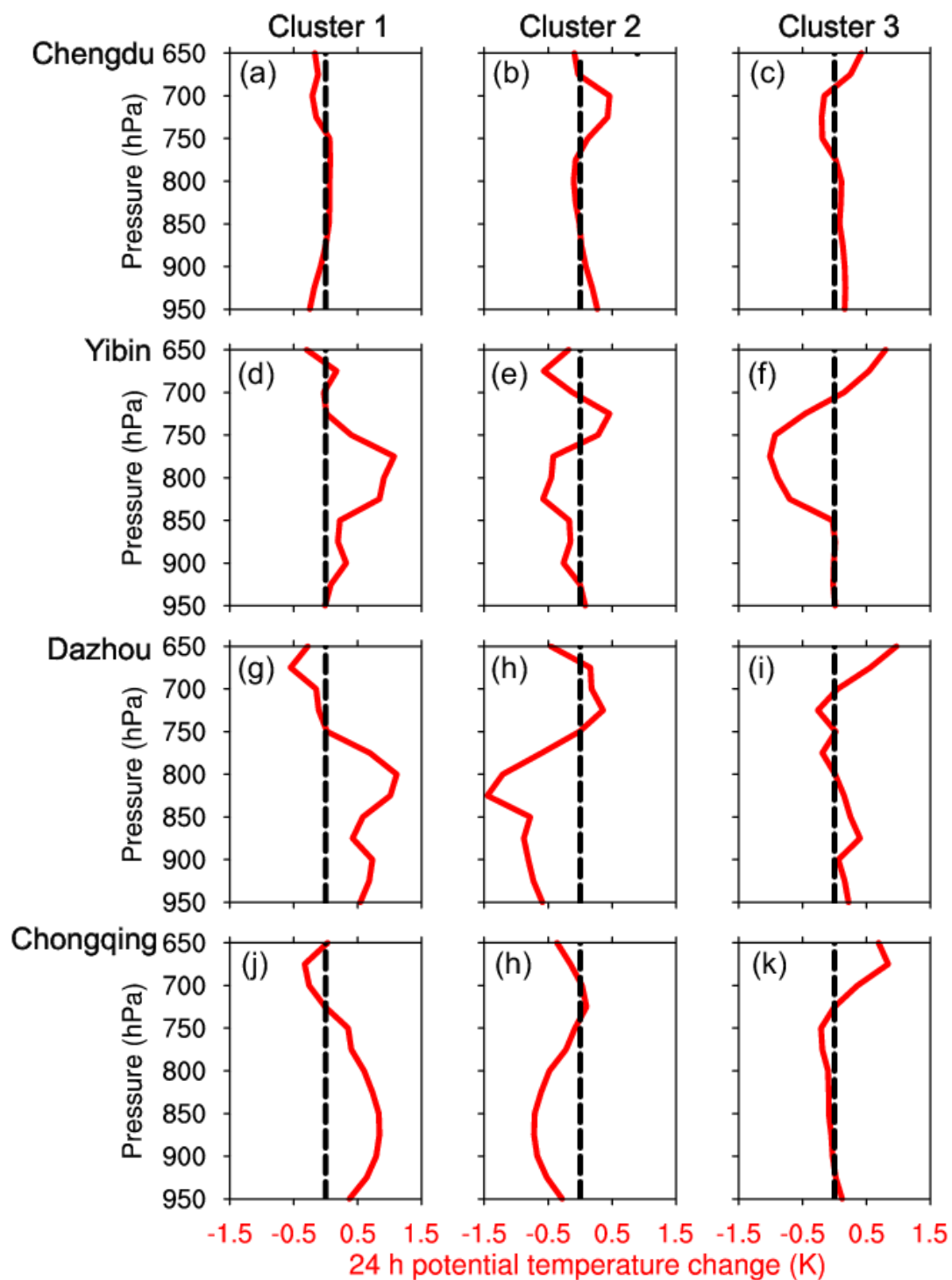
483

484 **Figure 4** Spatial distribution of the day-to-day changes in surface $PM_{2.5}$ (a–c) and PM_{10} (d–f) concentrations following the
485 three diurnal cycles within one day.

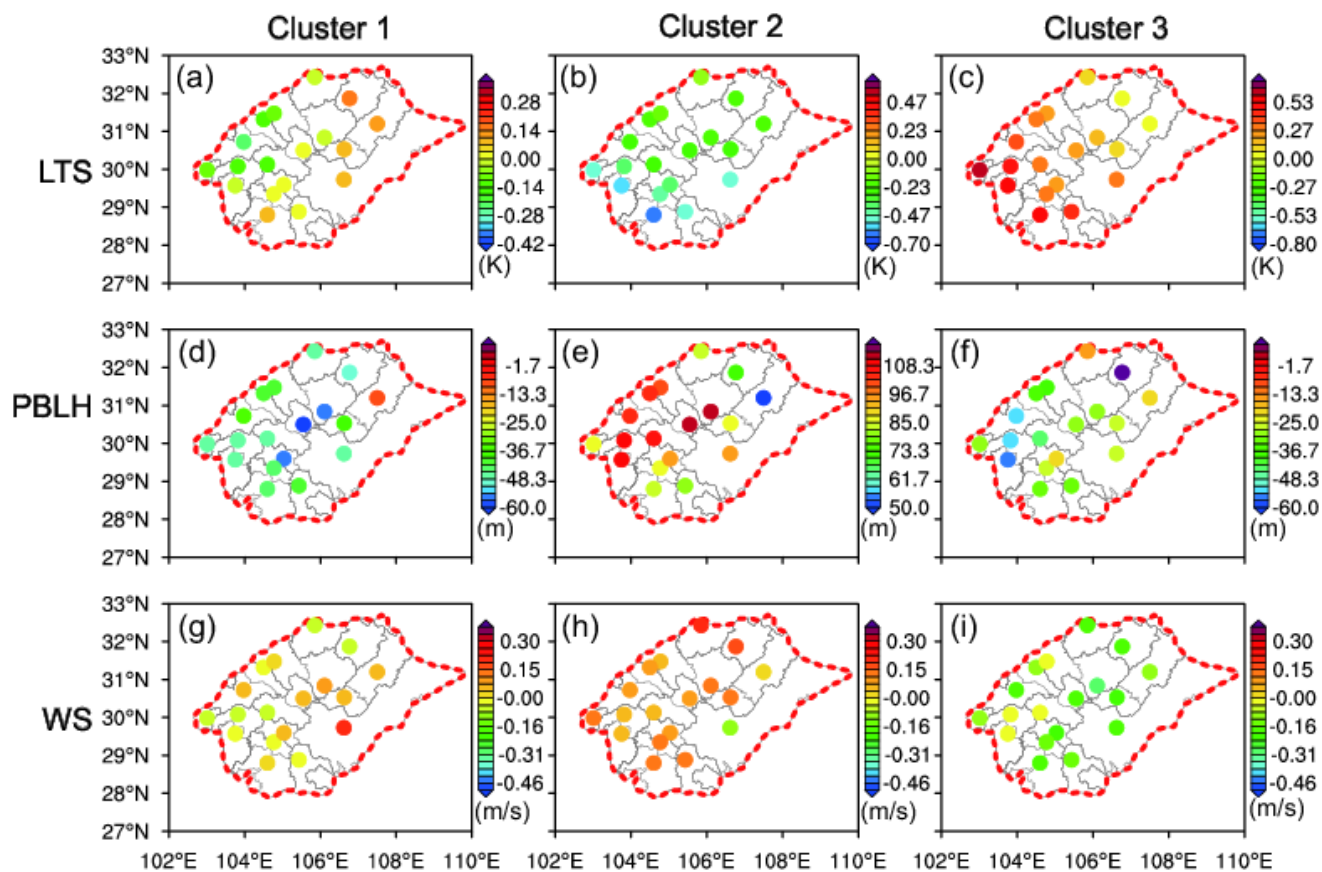


486

487 **Figure 5** Spatial distribution of the day-to-day changes in surface SO₂ (a–c), NO₂ (d–f), and CO (g–i) concentrations
488 following the three identified diurnal cycles within one day.



489
490 **Figure 6** Day-to-day changes in the PT vertical profiles at 20:00 BJT following the three identified diurnal cycles within one
491 day at four sounding stations. Chengdu (a–c), Yibin (d–f), Dazhou (g–i), and Chongqing (j–l).



492
493 **Figure 7** Spatial distribution of the day-to-day changes in LTS (a–c), PBLH (d–f), and WS (g–i)
494 identified diurnal cycles within one day.

495
496